https://doi.org/10.31925/farmacia.2026.4.6 **ORIGINAL ARTICLE**

OLEIC ACID DOUBLE-COATED Fe_3O_4-BASED MAGNETIC COLLOIDAL SUSPENSION INDUCES DOSE-DEPENDENT CYTOTOXICITY AND MITOCHONDRIAL DYSFUNCTION IN HEPG2 CELLS

SIMONA GEORGETA RADUȚ (MIHART) [1#], AURELIA GABRIELA ANTAL [2,3#], CAMELIA NICOLESCU [1]*, VLAD SOCOLIUC [4,5], ROBERT IANOȘ [6], IASMINA-ALEXANDRA PREDESCU [1,7,8], DIANA HAJ ALI [1,7,8], CRISTINA-ADRIANA DEHELEAN [7,8], LAURA SBÂRCEA [7,9,10], ELENA-ALINA MOACĂ [7,8]

[1]*Doctoral School, "Victor Babeș" University of Medicine and Pharmacy Timișoara, 2 Eftimie Murgu Square, 300041, Timișoara, Romania*
[2]*Research Centre for Experimental Pharmacology and Drug Design (X-Pharm Design), "Victor Babeș" University of Medicine and Pharmacy Timișoara, 2 Eftimie Murgu Square, 300041, Timișoara, Romania*
[3]*Department of Pharmacology-Pharmacotherapy, Faculty of Pharmacy, "Victor Babeș" University of Medicine and Pharmacy Timișoara, 2 Eftimie Murgu Square, 300041 Timișoara, Romania*
[4]*Laboratory of Magnetic Fluids, Center for Fundamental and Advanced Technical Research, Romanian Academy - Timișoara Branch, 24 M. Viteazu Avenue, 300223, Timișoara, Romania*
[5]*Research Center for Complex Fluids Systems Engineering, Politehnica University of Timișoara, 1 M. Viteazu Avenue, 300222, Timișoara, Romania*
[6]*Faculty of Chemical Engineering, Biotechnologies and Environmental Protection, Politehnica University Timișoara, 6 Vasile Pârvan Boulevard, 300223, Timișoara, Romania*
[7]*Faculty of Pharmacy, "Victor Babeș", University of Medicine and Pharmacy Timișoara, 2 Eftimie Murgu Square, 300041, Timișoara, Romania*
[8]*Research Centre for Pharmaco-Toxicological Evaluation, "Victor Babeș", University of Medicine and Pharmacy Timișoara, 2 Eftimie Murgu Square, 300041, Timișoara, Romania*
[9]*Department of Drug Analysis, Faculty of Pharmacy, "Victor Babeș" University of Medicine and Pharmacy Timișoara, 2 Eftimie Murgu Square, 300041, Timișoara, Romania*
[10]*Advanced Instrumental Screening Center, Faculty of Pharmacy, Victor Babeș University of Medicine and Pharmacy Timișoara, 2 Eftimie Murgu Square, 300041, Timișoara, Romania*

**corresponding author: camelia.lupou@umft.ro*
[#]Authors with equal contribution.

Manuscript received: April 2026

Abstract

The present study aimed to characterize the physicochemical properties and evaluate the *in vitro* cytotoxic effects of a magnetic colloidal suspension (MCS@OA/PBS) based on Fe_3O_4 nanoparticles coated with a double layer of oleic acid and dispersed in phosphate-buffered saline. Physicochemical characterization revealed magnetic behavior suitable for biomedical applications, a hydrodynamic diameter of approximately 46.6 nm, and satisfactory colloidal stability. Assessment of cytotoxic effects on the HepG2 cell line demonstrated a concentration-dependent response, characterized by decreased cell viability, impaired lysosomal integrity, nuclear morphological changes, and compromised mitochondrial membrane integrity and potential. These results support the preliminary potential of MCS@OA/PBS as a nanoplatform with possible future applications in the treatment of hepatocellular carcinoma.

Rezumat

În studiul de față a avut ca obiectiv caracterizarea fizico-chimică și evaluarea *in vitro* a efectelor citotoxice ale unei suspensii coloidale magnetice (MCS@OA/PBS), pe bază de nanoparticule de Fe_3O_4 acoperite cu un dublu strat de acid oleic și dispersate în soluție salină tamponată cu fosfați. Caracterizarea fizico-chimică a evidențiat un comportament magnetic adecvat pentru aplicații biomedicale, un diametru hidrodinamic de aproximativ 46,6 nm și o stabilitate coloidală satisfăcătoare. Evaluarea efectelor citotoxice asupra liniei celulare HepG2 a demonstrat un răspuns dependent de concentrație, caracterizat prin scăderea viabilității celulare, alterarea integrității lizozomale, apariția modificărilor morfologice nucleare și afectarea integrității și a potențialului membranei mitocondriale. Aceste rezultate susțin potențialul preliminar al MCS@OA/PBS ca nanoplatformă cu posibile aplicații viitoare în terapia carcinomului hepatocelular.

Keywords: Fe_3O_4 nanoparticles, magnetic colloidal suspension, hepatocellular carcinoma, cytotoxicity

Introduction

The incidence of mortality caused by liver cancer is one of the highest in the world, given its high incidence and poor prognosis. According to the latest GLOBOCAN 2022 statistics, liver cancer occupies the sixth place worldwide in terms of cancer prevalence, with approximately 866,136 new cases diagnosed every year. At the same time, it is the third leading cause of death, accounting for approximately 758,725 deaths yearly. In Europe, liver cancer is estimated to have led to approximately 91,000 new cases and over 82,000 deaths, continuing to be a significant cause of morbidity and mortality associated with cancer (1). Hepatocellular carcinoma (HCC), the most frequent form of liver cancer, is of both infectious and noninfectious origin. This is linked to infection with hepatitis B and C viruses, long-term alcohol consumption, metabolic diseases, and chronic liver disorders like cirrhosis and steatohepatitis (2).

The treatment of hepatocellular carcinoma still poses a significant challenge, especially since the disease is usually diagnosed at advanced stages, when the prognosis is unfavorable, and treatment options are limited. Even though targeted therapies and immunotherapy have improved disease outcomes, survival rates remain modest due to the emergence of treatment resistance and limited access to modern therapies in many healthcare systems (3). Nanotechnology may therefore constitute a valuable strategy for optimizing the treatment of hepatocellular carcinoma. Due to their small size and characteristic properties, nanoparticles have been extensively investigated as drug delivery systems in chemotherapy, with the potential to improve treatment outcomes, reduce side effects, and overcome drug resistance (4). In general, nanoparticles and Magnetic nanoparticles (MNPs) have sizes between 1 and 100 nm. They are distinguished by a high surface-to-volume ratio, giving them a number of unique physicochemical and biological properties. Because of these properties, nanoparticles can interact easily with cells and their organelles. This offers potential for their use in biomedical applications, such as targeted drug delivery and anticancer therapy (5-8).

Among the different types of iron oxide nanoparticles, magnetite (Fe_3O_4) and maghemite (γ-Fe_2O_3) have attracted considerable attention for their favorable magnetic properties and potential applications in drug delivery. This makes magnetic nanoparticles promising candidates for the targeted administration of bioactive compounds (9-11). Their biological activity is affected by particle size, surface properties, concentration, and coating, underscoring the need for detailed physicochemical characterization and biocompatibility evaluation before biomedical application.

Therefore, the present study aimed to investigate the *in vitro* biological activity of a biocompatible magnetic colloidal suspension (MCS) based on MNPs double-layer coated with 65-88% oleic acid (OA) and dispersed in phosphate buffer saline solution (PBS), against the HepG2 human hepatocellular carcinoma cell line by assessing cell viability, cellular and nuclear morphology, mitochondrial morphology, and membrane potential. Before being subjected to biological testing, the magnetic colloidal suspension was characterized by magnetic measurements and hydrodynamic diameter measurements *via* dynamic light scattering (DLS). In addition, to investigate the stability of the biocompatible MCS, the Zeta potential was determined. These preliminary physicochemical analyses were performed to assess whether the MCS@OA/PBS formulation possesses suitable magnetic and colloidal properties for future biomedical applications.

Materials and Methods

Synthesis and Characterization of Magnetic colloidal suspension (MCS)

For the synthesis of MCS it was used the Fe_3O_4 magnetic nanopowder originated from the exact batch previously designated by Ianoș *et al*. (12). The magnetic nanoparticles (MNPs) of iron oxide were used, fabricated by the combustion method, starting from $Fe(NO_3)_3 \times 9\ H_2O$, purchased from Carl Roth, Germany, used as an oxidizer agent, and glucose (D-(+)-$C_6H_{12}O_6$, purchased from Riedel-de Haën, Germany), used as a fuel, and the reaction was conducted in the absence of air. The structural, surface, and magnetic properties of the MNPs were previously characterized by X-ray diffraction (XRD), X-ray photoelectron spectroscopy (XPS), Brunauer–Emmett–Teller (BET) surface-area analysis, and vibrating-sample magnetometry. XRD identified Fe_3O_4 as the crystalline phase and indicated an average crystallite size of approximately 10 nm, whereas the previously reported BET specific surface area was 106 m^2/g, equivalent particle diameter - approximately 11 nm, and saturation magnetization was 55.3 emu/g, respectively. For the present investigation, the synthesized nanopowder batch was double-layer coated with 65-88% oleic acid ($C_{18}H_{34}O_2$, from Merck, Germany) (13) and dispersed in phosphate-buffered saline (PBS), according to the detailed protocol previously described (14). After synthesizing the as-denoted MCS@OA/PBS sample, its saturation magnetization was determined using a VSM 880 vibrating-sample magnetometer (DMS/ADE Technologies, Westwood, MA, USA). The density of the MCS@OA/PBS suspension was measured at 25 °C using a DMA 35 portable density meter (Anton Paar GmbH, Graz, Austria). The Fe_3O_4 concentration of the MCS@OA/PBS suspension was estimated from its

saturation magnetization using the proportional relationship between the saturation magnetization of a magnetic colloidal suspension and the magnetic-particle volume fraction (15):

$$M_s = M_d \cdot \varphi$$

Where M_S is the saturation magnetization of the magnetic colloidal suspension, expressed in Gs; M_d is the saturation magnetization *per* unit volume of the dispersed magnetic solid phase, expressed in Gs; and φ is the dimensionless magnetic-particle volume fraction.

Consequently, the magnetic-particle volume fraction was calculated as follows:

$$\varphi = \frac{M_s}{M_d}$$

Based on previously reported calibration data for magnetite-based magnetic fluids, according to which a magnetic-particle volume fraction of 0.07 corresponds to a saturation magnetization of approximately 300 Gs (13), the effective M_d value used in the calculation was approximately 4.29×10^3 Gs. The Fe_3O_4 mass concentration was subsequently calculated according to the following relationship:

$$C_{Fe_3O_4} = \varphi \cdot \rho_{Fe_3O_4}$$

where $\rho_{Fe_3O_4}$ is the theoretical density of magnetite, taken as 5.2 g/cm^3. The resulting concentration was expressed as mg of Fe3O4 *per* mL of magnetic colloidal suspension and was subsequently used to prepare the working concentrations for the biological assays.

The hydrodynamic diameter of the sample was investigated by dynamic light scattering (DLS), using a ZetaSizer NanoZS from Malvern Instruments (Worcestershire, UK). The zeta potential of the sample was determined by electrophoretic light scattering using the same ZetaSizer NanoZS instrument. In addition, before the biological assays, the morphology of the MCS@OA/PBS formulation was investigated by bright-field scanning transmission electron microscopy (STEM) using an HD-2300 scanning transmission electron microscope (Hitachi High-Technologies Corporation, Tokyo, Japan) operated at 200 kV. Images were acquired using the transmitted-electron detector at magnifications of ×150,000 and ×600,000. The elemental distribution of carbon, iron, and oxygen was investigated by energy-dispersive X-ray spectroscopy (EDS) coupled to the microscope.

Reagents and Instruments used for in vitro assays

The MTT reagent (3-(4,5-dimethylthiazol-2-yl)-2,5-diphenyltetrazolium bromide) was purchased from Roche Holding AG (Basel, Switzerland). Hoechst 33342 and MitoTracker™ Red CMXRos fluorescent dyes were supplied by Thermo Fisher Scientific (Waltham, MA, USA), whereas the JC-1 Mitochondrial Membrane Potential Assay Kit was obtained from Elabscience (Houston, TX, USA). Cell culture reagents, including Eagle's Minimum Essential Medium (EMEM, 30-2003™), fetal bovine serum (FBS), and a penicillin–streptomycin solution, were purchased from ATCC (American Type Culture Collection, Lomianki, Poland). The Cytation 5 multimode plate reader, Lionheart FX automated microscope, and Gen5™ Microplate Data Collection and Analysis Software (Version 3.14) were provided by BioTek Instruments (Winooski, VT, USA).

Cell Line and Culture Conditions

HepG2 cells, obtained from human hepatocellular carcinoma (HB-8065™; ATCC, Manassas, VA, USA), were cultivated in the specific medium (EMEM), supplied with FBS (10%) alongside an antibiotic solution (1%), and placed at 37 °C in a humidified atmosphere with 5% CO_2. The MCS@OA/PBS stock magnetic colloidal suspension, containing an Fe_3O_4 concentration of approximately 3.24 mg/mL, was diluted in complete EMEM culture medium immediately before each experiment to prepare the working suspensions. The concentrations reported throughout the study (10, 100, 200, 300, and 400 µg/mL) refer to the estimated final Fe_3O_4 concentration in the culture medium. These concentrations corresponded to stock suspension additions of approximately 0.31%, 3.09%, 6.17%, 9.26%, and 12.35% (v/v), respectively. HepG2 cells were exposed to the treatment suspensions for 24 h.

Cell Viability Assessment

The first step in investigating cytotoxic effects was assessing cell viability using the MTT colorimetric assay (16). HepG2 cells were seeded in 96-well plates at a density of 1×10^4 cells/well and allowed to attach and grow until they reached approximately 70% confluence. The cells were then treated with the MCS@OA/PBS sample at concentrations of 10, 100, 200, 300, and 400 µg/mL and incubated for 24 h. After incubation, the culture medium was replaced with fresh media, and 10 µL of MTT reagent was added to each well. The plates were incubated for another 3 h at 37 °C in a humidified atmosphere containing 5% CO_2. After the incubation, 100 µL of MTT solubilization solution was added to each well, and the plates were incubated in the dark at room temperature for 30 min. Finally, absorbance was measured at 570 nm with background correction at 630 nm using a Cytation™ 5 microplate reader.

Cell Morphology Assessment

Treatment-induced morphological changes in HepG2 cells were examined by bright-field microscopy. The cells were plated in 96-well plates, and once they reached the desired confluence (70%), they were treated with the MCS@OA/PBS sample at concentrations of 10, 100, 200, 300, and 400 µg/mL for 24 h. Finally, a Lionheart FX automated microscope was used to capture representative images to observe morphological changes (17, 18).

Neutral Red Staining and Uptake

Afterward, the neutral red uptake assay was performed as described in the protocol by Marcovici *et al*. (19). HepG2 cells were seeded in 96-well plates at a density of 1×10^4 cells/well. When the desired confluence was achieved (70%), they were treated with MCS@OA/PBS (10, 100, 200, 300, and 400 µg/mL) for 24 h. At the end of the treatment, the culture medium was replaced with a medium containing neutral red (40 µg/mL; 100 µL/well). After incubation for 2 h at 37 °C in a humidified atmosphere containing 5% CO_2, excess dye was rinsed thoroughly with PBS. Afterward, morphological properties were observed using a Lionheart FX automated brightfield microscope. The intracellular stored dye was eliminated by adding 150 µL of a neutral red destain solution (50% of 96% ethanol, 49% ultrapure deionized water, and 1% glacial acetic acid)well. A 10-minute shaking period was then performed to extract the dye from the cells. The absorbance reading was performed at 540 nm using the Cytation 5 multimodal reader.

Mitochondria and Nuclei Staining

Mitochondrial and nuclear morphology were assessed after treating HepG2 cells with the MCS@OA/PBS sample. The cells were seeded in 12-well plates (1×10^5 cells/well), and when they reached 70% confluence, the cells were treated with the sample at concentrations ranging from 10 to 400 µg/mL for 24 h. To visualize the mitochondrial network, a 1 mM stock solution of MitoTracker prepared in DMSO was diluted in complete culture medium to obtain a final working concentration of 300 nM. The cells were incubated with the staining solution for 30 min, and the excess dye was removed by washing with a new fresh culture medium. The cells were fixed with 4% paraformaldehyde for 10 min at RT and washed again with PBS. The nuclear morphology was evaluated by Hoechst 33342 staining. Following fixation, cells were incubated with Hoechst 33342 diluted 1:2000 in PBS for 5–10 min in the absence of light. After staining, the solution was discarded, and the wells were washed three times with PBS to eliminate unbound dye. Fluorescence images representative of each experimental condition were acquired at 20× magnification using a Lionheart FX automated microscope. A similar protocol was described by Nica *et al*. (20**).**

JC-1 staining

To evaluate the effects of the MCS@OA/PBS sample (10-400 µg/mL) on mitochondrial membrane potential ($\Delta\Psi m$) in HepG2 cells, a test based on the fluorescent dye JC-1 was used. Cells were plated in black-walled, clear-bottom 96-well plates (1×10^4 cells/well), and when the cells were ~70% confluent, cells were treated with the sample for 24 h. At the end of the treatment, the media was removed, and cells were gently washed with PBS. Cells were incubated with JC-1 solution (5 µM, 100 µL/well) for 45 min at 37 °C, and cells were washed twice with PBS to remove excess dye. Fluorescent images were captured using the Lionheart FX automated microscope, and the fluorescence intensities of JC-1 aggregates (red fluorescence; emission at 590 nm) and JC-1 monomers (green fluorescence; emission at 529 nm) were measured using the Cytation 5 reader (21).

Statistical Analysis

All experiments were performed in triplicate, and the results are presented as mean ± standard deviation (SD). Statistical analysis was performed using GraphPad Prism software (version 11.0.2; GraphPad Software, San Diego, CA, USA). Differences between the control and treated groups were analyzed using one-way analysis of variance (ANOVA), followed by Dunnett's multiple comparisons test. Differences were considered statistically significant at $p < 0.05$ and are indicated as follows: *$p < 0.05$, **$p < 0.01$, ***$p < 0.001$, and ****$p < 0.0001$.

Results and Discussion

HCC remains a major therapeutic challenge due to its poor prognosis and the limitations of current treatment strategies. Nanotechnology has become a promising strategy for optimizing the delivery and therapeutic effectiveness of anticancer medicines (22). In this context, the present study aimed to investigate the magnetic properties, hydrodynamic diameter, and zeta potential, as well as the *in vitro* biological effects of a magnetic colloidal suspension based on magnetic nanoparticles obtained through the combustion method, double-layer coated with oleic acid and dispersed in PBS (MCS@OA/PBS) to explore their potential for future biomedical applications in hepatic cancer. To achieve this, the study was structured in two stages: (a) a preliminary physicochemical characterization of the synthesized MCS@OA/PBS sample and (b) evaluation of their biological activity in the HepG2 human hepatocellular carcinoma cell line by assessing cell viability, nuclear and mitochondrial morphology, and mitochondrial membrane potential.

The HepG2 cell line was selected due to its widespread use in the scientific literature and its application as an *in vitro* model for cytotoxicity studies. These cells are isolated from HCC, the most common form of liver cancer, and exhibit a considerable degree of genetic and morphological similarity to HCC-derived tissues. These characteristics make HepG2 cells a proven and reliable model for investigating the cytotoxic effects of new types of compounds (23). The concentrations selected in the present study were based on previously published reports investigating the biological effects of MNPs (Fe_3O_4 and γ-Fe_2O_3) in different cancer cell models (9,24).

Preliminary Physicochemical Characterization

The density of the MCS@OA/PBS suspension measured at 25 °C was 1.0141 g/cm^3. The density measurement was treated as an independent physicochemical descriptor and was not used to quantify the magnetic phase because it includes contributions from the aqueous carrier and the oleic acid coating. The saturation magnetization of the suspension was 2.667 Gs. Based on the calibration relationship described in the Materials and Methods section, this value corresponded to a magnetic-particle volume fraction of 6.23×10^{-4}. Considering the theoretical density of magnetite, the Fe_3O_4 concentration of the MCS@OA/PBS suspension was estimated at approximately 3.24 mg/mL. This concentration was used to prepare the working suspensions employed in the biological assays.

The magnetization curve of the MCS@OA/PBS system (Figure 1) shows a rapidly rising magnetization at the low applied magnetic fields, then a gradual rise up to saturation. The saturation magnetization measurement for the magnetic colloidal suspension was 2.667 Gs, with about 95% of this value reached at an applied field of approximately 2.414 kOe. This indicates that the magnetic nanoparticles maintain a distinct magnetic response after double coating with oleic acid and dispersion in PBS. The relatively low value of magnetization is likely due to a dilute colloidal system that contains a substantial nonmagnetic fraction composed of the aqueous medium and the organic coating. Because the measurement represents a virgin magnetization curve rather than a complete hysteresis loop, the value observed near zero applied field should not be interpreted as evidence of negligible remanence or superparamagnetic behavior. Consequently, remanent magnetization, coercivity, blocking behavior, and the magnetic classification of the MCS@OA/PBS formulation could not be established from the available data.

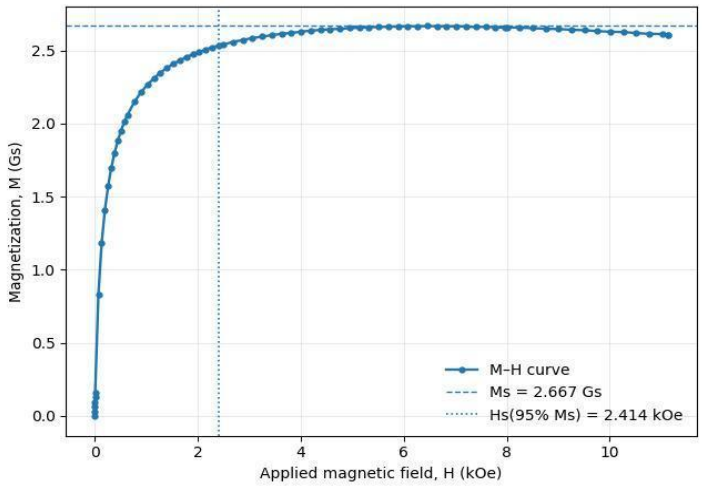

Figure 1.
Magnetization curve of the MCS@OA/PBS sample based on Fe_3O_4-NPs coated with a double layer of 65-88% oleic acid and dispersed in PBS

Within the framework mentioned above, the saturated magnetization observed for the MCS@OA/PBS sample indicates that the Fe_3O_4 nanoparticles retained their magnetic reactivity even after being coated with a second layer of oleic acid and dispersed in PBS. Despite being lower than the saturation magnetization reported for bulk Fe_3O_4 or for dry magnetic nanoparticles (MNPs), the value is anticipated for a dilute colloidal suspension, where the magnetic phase is dispersed in a nonmagnetic aqueous vehicle and surrounded by an organic stabilizing layer (14).

Dynamic light scattering analysis yielded a Z-average hydrodynamic diameter of 46.62 nm and a polydispersity index (PDI) of 0.230 for the MCS@OA/PBS formulation, indicating a moderately polydisperse colloidal system. The Z-average and PDI were considered the primary DLS parameters. The intensity-weighted distribution showed a dominant nanoscale peak centered at approximately 58.06 nm, whereas the volume-weighted distribution showed a principal peak at approximately 30.76 nm. However, these values were treated as complementary distribution outputs and were not directly compared with the Z-average because they are derived using different weighting and data-transformation approaches. An additional signal was detected in the micrometric range. Because particles of approximately 4.1 - 4.6 µm approach or exceed the practically reliable range of DLS measurements and may violate the assumption of negligible sedimentation, this signal was not interpreted quantitatively as a distinct particle population. Instead, it was considered a possible measurement artifact caused by transient aggregates, dust contamination, or sedimentation during analysis. Before the biological assays, the MCS@OA/PBS

formulation was filtered through a 0.22 µm membrane to reduce the presence of residual large particulate material.

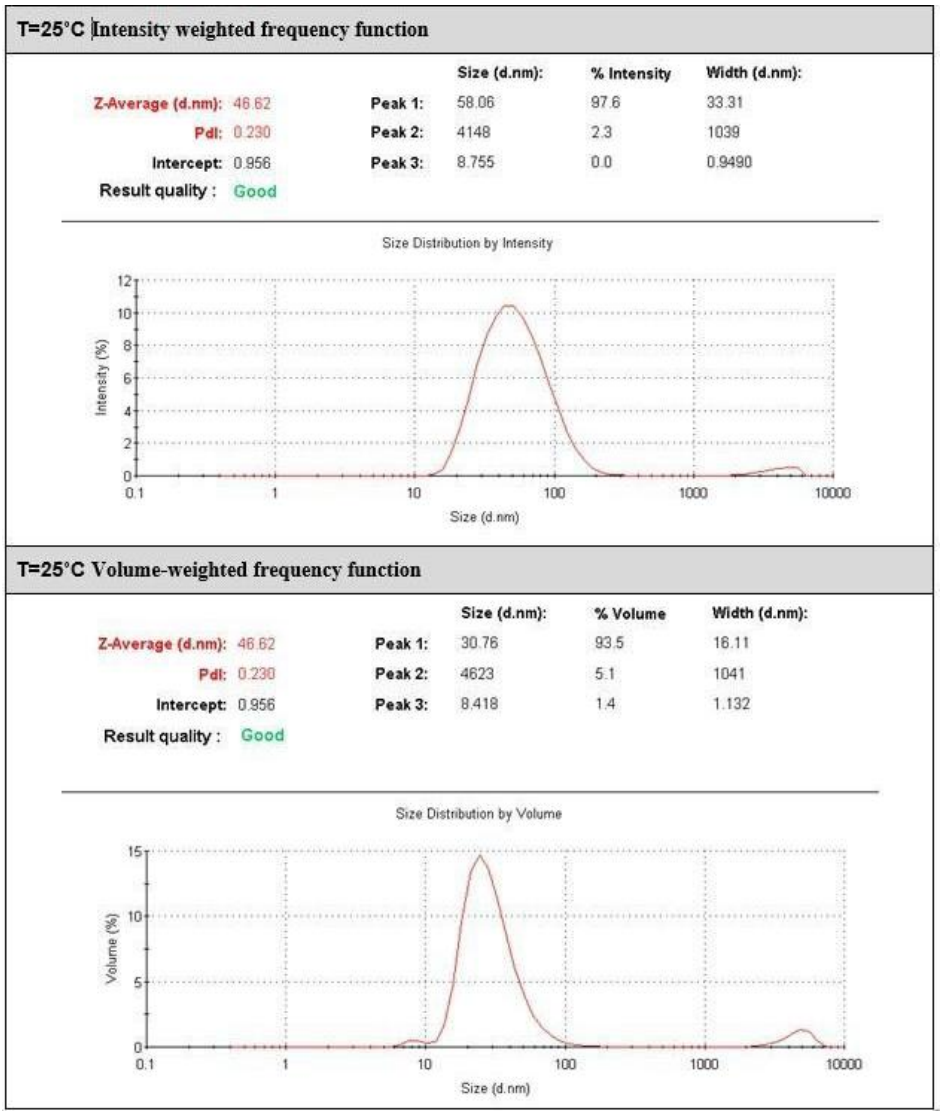

Figure 2.
The size distribution of the MCS@OA/PBS sample based on Fe_3O_4-NPs coated with a double layer of 65-88% oleic acid and dispersed in PBS – A) by intensity and B) by volume

The zeta potential value of −28.7 mV indicates a moderately high negative surface charge and suggests moderate to good electrokinetic stability. Although the value is slightly below the commonly considered ±30 mV threshold for highly electrostatically stabilized dispersions, it is important to consider that the measurement was performed in PBS, where the ionic strength may partially screen the surface charge. Therefore, the colloidal stability of this formulation is likely supported not only by electrostatic repulsion, but also by steric stabilization provided by the oleic acid coating.

Based on the results obtained, one can affirm that our findings are in accordance with scientific literature, data showing that a magnetic colloidal suspension, based on oleic acid-coated Fe_3O_4-NPs, can exhibit hydrodynamic diameters below 100 nm (25-27), a size interval that is suitable for applications in biomedicine, including drug delivery vectors, MRI contrast agents, and hyperthermia-related approaches (28-30). The apparent micrometric signal detected by DLS was not considered a reliably quantified particle population due to the technique's limitations with large, potentially sedimenting structures. Such signals may arise from occasional aggregates, dust particles, or transient scattering events and should therefore be interpreted cautiously. The PDI value of 0.230 indicates moderate, rather than low, polydispersity, suggesting that the formulation is predominantly nanoscale but not strictly monodisperse

(28,30). Unlike previously reported magnetic colloidal systems, in which higher PDI values were associated with greater distributions, coating heterogeneity, or partially aggregated particles, the PDI value obtained in the present study indicates moderate heterogeneity of the colloidal formulation and does not exclude the presence of aggregates (31–33).

The primary particles were predominantly within the nanometric range and appeared to have dimensions of approximately 10–20 nm (Figure 3A, B). STEM examination revealed electron-dense, approximately rounded to slightly irregular primary particles arranged in small clusters. These dimensions are consistent with the previous characterization of the exact precursor nanopowder batch, for which XRD and BET-derived dimensions of approximately 10 and 11 nm, respectively, were reported (12), and with TEM studies describing oleic-acid-coated magnetite nanoparticles with dimensions of 7 and 19 nm (34).

The STEM–EDS maps showed spatial co-localization of Fe and O within the particle-rich region, supporting an iron-oxide-based composition (Figure 3C), in agreement with elemental analyses reported for other Fe_3O_4-based nanosystems (35). Nevertheless, EDS does not differentiate between crystalline iron-oxide phases, and the carbon signal may originate from both the oleic acid coating and the carbonaceous support, so it was not considered direct evidence of coating formation.

Overall, based on its measured physicochemical characteristics, the MCS@OA/PBS formulation was subsequently evaluated for its biological effects in HepG2 cells.

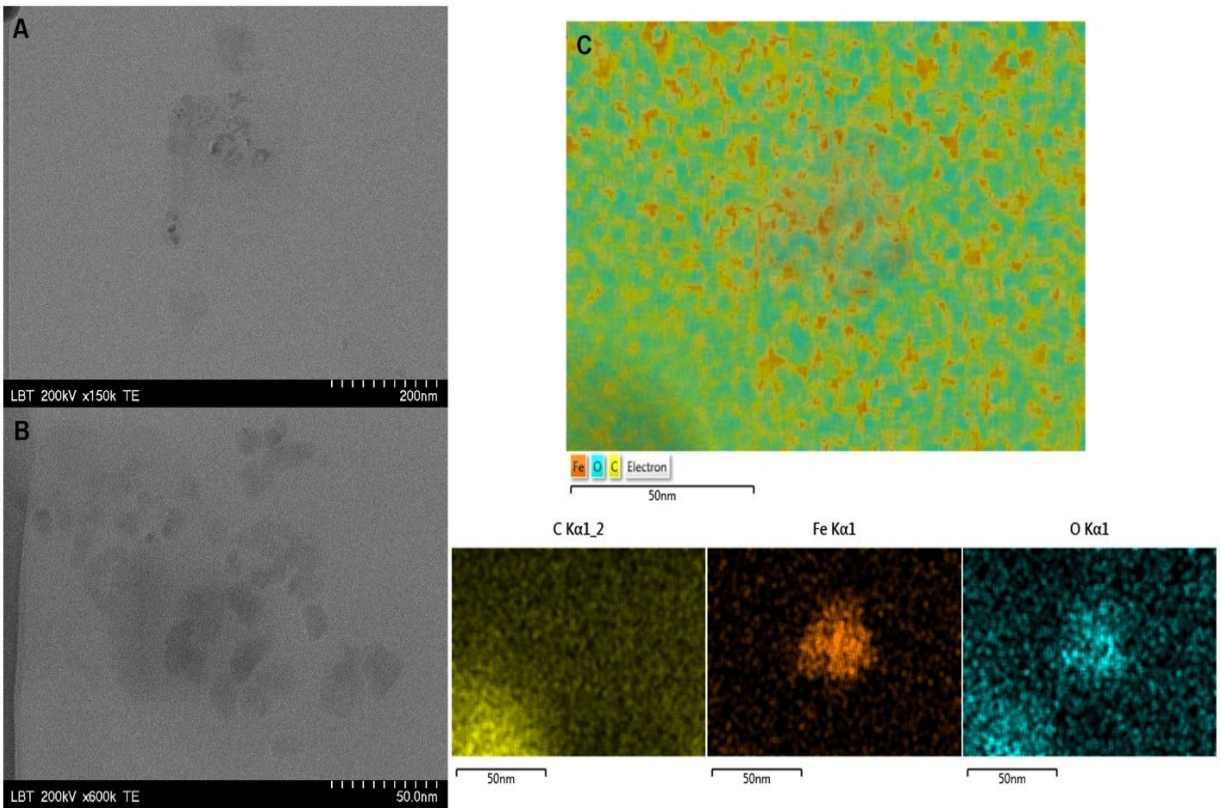

Figure 3.

STEM imaging and EDS elemental mapping of the MCS@OA/PBS formulation. (A) Representative bright-field STEM image acquired at ×150,000 magnification; scale bar: 200 nm. (B) Higher-magnification bright-field STEM image acquired at ×600,000 magnification; scale bar: 50 nm. (C) STEM–EDS elemental mapping, including the merged C/Fe/O distribution and the individual C, Fe, and O maps.

Cell Viability Assessment

First, the cytotoxicity of MCS@OA/PBS on the HepG2 cell line was evaluated by measuring the effect of MCS@OA/PBS on cell viability after 24 h treatment. The MTT assay (Figure 4) indicated that cell viability decreased in a concentration-dependent manner for all concentrations. At the lowest concentration of 10 µg/mL, the cell viability was similar to the untreated control group (99.37%). The cell viability was significantly reduced to 21.60%, 11.24%, 5.28% and 5.27% at concentrations of 100 µg/mL, 200 µg/mL, 300 µg/mL and 400 µg/mL, respectively.

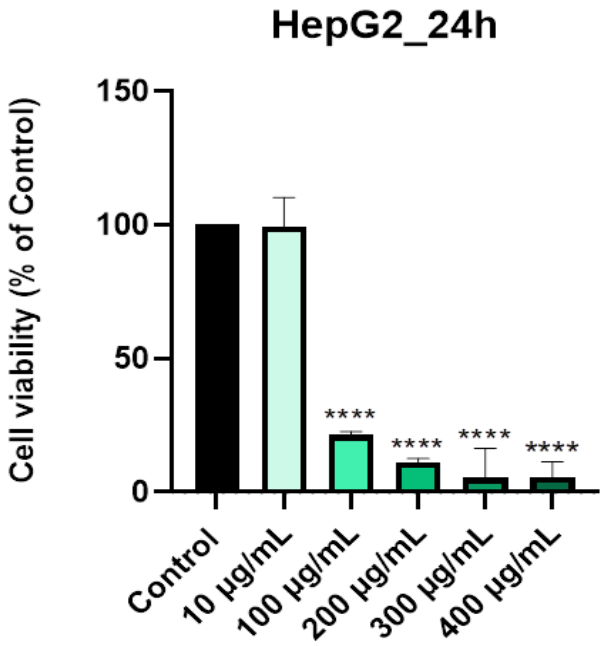

Figure 4.

Graphical illustration of cell viability following the exposure of HepG2 cells to the MCS@OA/PBS sample based on Fe_3O_4-NPs coated with a double layer of oleic acid and dispersed in PBS, at concentrations ranging from 10 to 400 µg/mL. Cell viability was expressed as a percentage relative to the untreated control. Data are presented as the mean ± standard deviation (SD). Statistical analysis was achieved using one-way analysis of variance (ANOVA), and then Dunnett's multiple comparison test was performed. Differences were considered statistically significant compared to the untreated control at the significance levels ****$p < 0.0001$

The MTT assay has become one of the most widely used methods for the initial assessment of cytotoxicity, as it provides an indirect measure of cell viability based on the metabolic activity of viable cells. The assay is dependent on the reduction of the tetrazolium salt MTT to insoluble violet formazan crystals by cells that are metabolically active; the quantity of formazan formed is related to the count of viable cells (36). In this study, MCS@OA/PBS produced a concentration-dependent cytotoxic effect. Cell viability was similar to that of the control group at 10 µg/mL. A remarkable decrease was reported at concentrations of 100 µg/mL and higher (Figure 4). These observations are aligned with prior reports indicating that the cytotoxicity of Fe_3O_4 nanoparticles increases with concentration, while lower concentrations, in general, possess lower toxicity in HepG2 cells (37). In other tumor cell lines, similar effects were observed. For example, magnetic nanoparticles analyzed on A549 and NCI-H460 lung cancer cells, at concentrations of 150, 300, and 500 µg/mL, applied for 24-96 hours, led to a gradual decrease in cell viability. A549 cells exhibited greater sensitivity to the treatment compared to NCI-H460 cells (9). Kai *et al*. studied the effect of Fe_3O_4 based magnetic nanoparticles on BEL-7402 hepatocellular carcinoma cells in a concentration range from 0.01 mg/mL to 2 mg/mL for 24 h. In this study, a decrease in cell viability was observed, which was concentration-dependent and more obvious at higher concentrations (38).

Cell Morphology Evaluation

Next, we evaluated the effect of MCS@OA/PBS on the morphology of HepG2 cells by observing morphological changes. Microscopic examination (Figure 5) showed that cells treated with 10 µg/mL of the MCS@OA/PBS sample for 24 h displayed a morphology similar to that of the control group, with a slight reduction in cell confluence. However, at concentrations of 100 µg/mL, the cell colonies were observed to be smaller and more fragmented. The individual cells were found to be structurally severely damaged, with the presence of abundant cellular debris. At the highest concentrations (300 and 400 µg/mL), the hallmark characteristics of HepG2 cell line colonies were almost totally lost, hinting at severe cytotoxic damage.

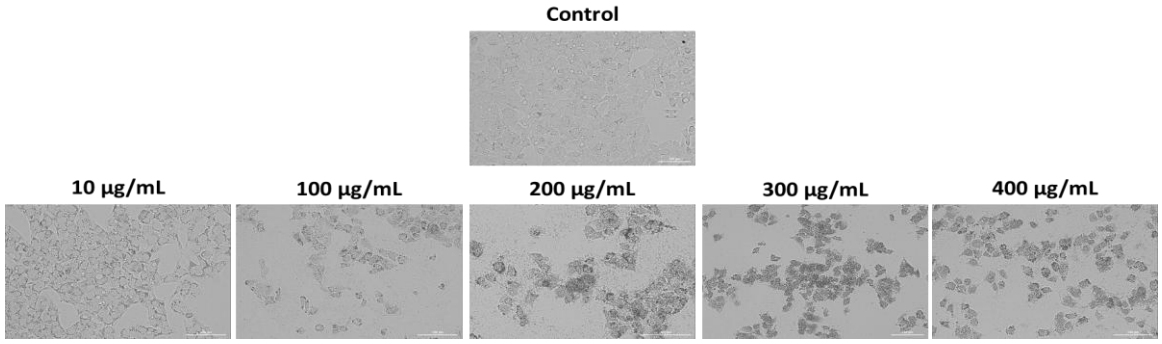

Figure 5.
Representative microscopic images of HepG2 cells following 24 h exposure to the MCS@OA/PBS sample based on Fe_3O_4-NPs coated with a double layer of oleic acid and dispersed in PBS at concentrations ranging from 10 to 400 µg/mL. Scale bar indicates 100 µm

Studies of the morphological appearance of cells after treatment are important for the cytotoxic evaluation of a test compound. These can provide details, including the type of cell death involved in the compound's effect (39). In untreated cells, HepG2 cells exhibit an adherent morphology, generally displaying the morphological characteristics of epithelial cell lines and forming compact colonies (40). In the present study, exposure of HepG2 cells to MCS@OA/PBS led to significant morphological changes. At the highest concentrations tested, the formation of HepG2 cell colonies (the characteristic feature of this cell line) mostly disappeared; also, intense cell fragmentation was noticed, suggesting strong cytotoxic effects. Prior studies have likewise indicated that exposure of HepG2 cells to Fe_3O_4 nanoparticles leads to considerable morphological changes. For example, Sathishkumar and colleagues examined the impact of Fe_3O_4 magnetic nanoparticles synthesized using Couroupita guianensis Aubl. fruit extract on HepG2 cells. At concentrations up to 250 µg/mL and after 24 hours of exposure, treated cells showed obvious morphological alterations. The changes consisted of loss of cytoplasmic membrane integrity, diminished cell confluence, and the formation of cell aggregates (41).

Neutral Red Staining and Uptake Assay

The next step involved evaluating the cytotoxic effects of the MCS@OA/PBS sample using a complementary cell viability assay. While the MTT assay determines viability based on mitochondrial metabolic activity, the neutral red uptake (NRU) assay assesses it by quantifying lysosomal integrity. Microscopic images in Figure 6A show that cells treated with 10 µg/mL of the sample had NRU similar to the untreated control. Conversely, cells treated with concentrations from 100 to 400 µg/mL showed almost no dye uptake and marked morphological changes, indicating severe loss of cellular integrity. These microscopic observations were supported by the quantitative NRU levels (Figure 6B). The percentages of NRU decreased to 82.37%, 14.59%, 8.91%, 5.86%, and 3.60% after treatment with MCS@OA/PBS at 10, 100, 200, 300, and 400 µg/mL, respectively. To summarize, these results show a pronounced, dose-dependent cytotoxic effect of the test sample and suggest that its toxicity is associated not only with impaired mitochondrial activity but also with significant lysosomal damage.

The NRU assay is a method frequently applied to estimate cell viability and cytotoxicity. The assay is dependent on the capacity of viable cells to take up the NRU dye into their lysosomes. Once the dye is extracted, its absorbance is determined sp-ectrophotometrically, allowing an estimate of the count of viable cells (42). Disruption of lysosomal functions is considered an important indicator of cell death, as impairment of lysosomal integrity and function is involved in both apoptosis and necrosis. In the case of apoptosis, lysosomal membrane permeabilization leads to the release of lysosomal proteases, which contribute to caspase activation and the initiation of the apoptotic cascade. In the case of necrosis, the massive release of lysosomal hydrolytic enzymes into the cytosol and the extracellular space leads to the degradation of cellular components and promotes cytosolic acidification, thereby amplifying cellular destruction (43). This study found that both microscopic examination and quantitative analysis suggest a significant decrease in intracellular dye uptake, indicating a severe disruption of lysosomal integrity. However, this assessment following treatment with different magnetic nanoparticles has also been reported. In this regard, Jędrzejczak-Silicka *et al.* examined the impact of graphene oxide–Fe_3O_4 nanoparticles on MCF-7 breast cancer cells after 24 hours of exposure to concentrations of up to 50 µg/mL. Similar to our study, the authors observed a significant reduction in the intracellular dye accumulation, indicating affected lysosomal integrity (44).

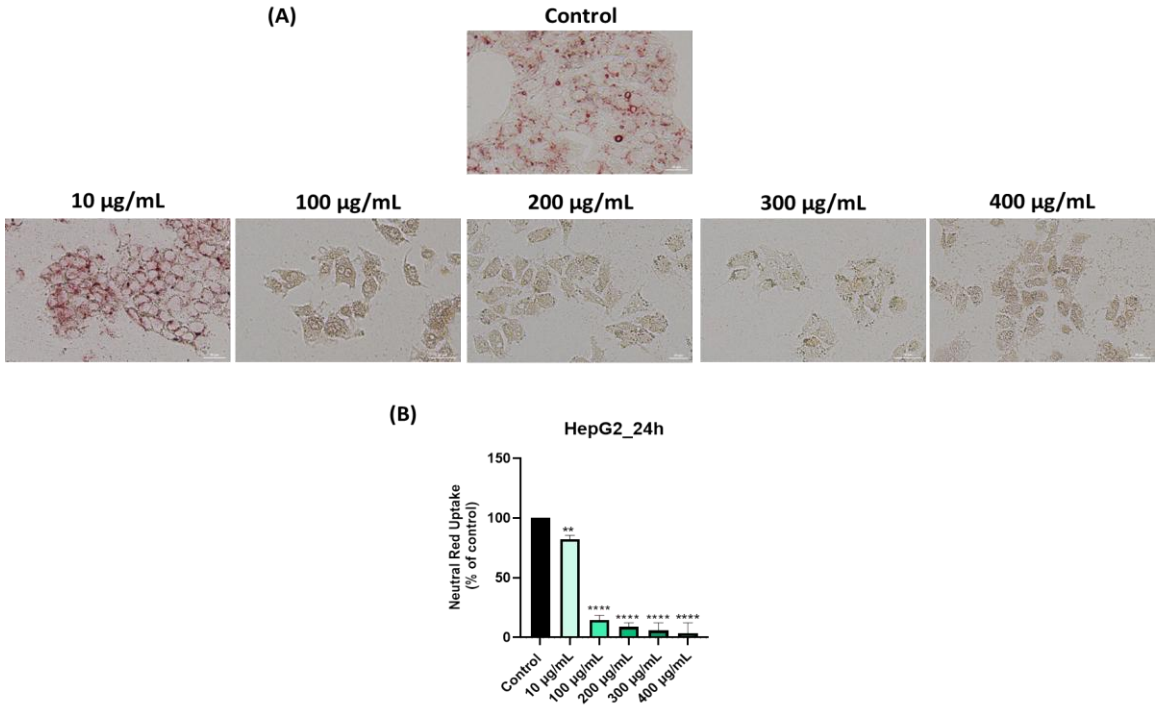

Figure 6.

Neutral Red Uptake (NRU) assay results. A) Representative microscopic images acquired following the NRU assay. Scale bar = 30 µm. B) Quantitative analysis of the NRU assay. Neutral Red Uptake was expressed as a percentage relative to the untreated control. Data are presented as the mean ± standard deviation (SD). Statistical analysis was performed using one-way analysis of variance (ANOVA), followed by Dunnett's multiple comparisons test. Differences were considered statistically significant compared to the untreated control at the significance levels ** $p < 0.01$ and ****$p < 0.0001$

Mitochondrial Membrane Potential (ΔΨm) Assessment Using Jc-1 Assay

Given the results obtained from previous cytotoxicity tests, the study was extended to examine the effects of the MCS@OA/PBS on mitochondrial membrane potential using the JC-1 assay. As shown in Figure 7, following treatment with the administered samples, the impairment of mitochondrial membrane potential was dose-dependent. Thus, compared to the control, at a concentration of 10 µg/mL, a slight decrease in red fluorescence and an increase in green fluorescence were observed compared to the control. These observations suggest that the polarity of the mitochondrial membrane was generally preserved at this concentration. In the case of treatment with 100 and 200 µg/mL, the cells exhibited predominantly yellow/orange fluorescence in the merged images. These findings suggest a partial loss of mitochondrial membrane potential. Exposure to concentrations of 300 and 400 µg/mL provoked a predominance of green fluorescence, along with a visible reduction in cell confluence. Furthermore, noticeable morphological changes were detected, corresponding to significant depolarization of the mitochondrial membrane. These qualitative observations were confirmed by quantitative analysis of the ratio between the fluorescence of JC-1 aggregates and that of monomers, as shown in Figure 7B. The ratio decreased progressively compared to the control group. Thus, the following percentages were recorded: 84.04%, 24.61%, 15.55%, 9.63%, and 5.42% for 10, 100, 200, 300, and 400 µg/mL of nanoparticles, respectively. Overall, the JC-1 assay revealed a clear, dose-dependent decline in the mitochondrial membrane potential of HepG2 cells. These results indicate progressive mitochondrial depolarization in response to exposure to the MCS@OA/PBS formulation.

Loss of mitochondrial membrane potential (ΔΨm) is a pivotal feature of the apoptotic process and an important marker of mitochondrial dysfunction. JC-1 is a cationic dye that is used to evaluate ΔΨm in viable and apoptotic cells. In intact cells with a relatively high ΔΨm, JC-1 is accumulated and localized in active mitochondria, where it forms red-fluorescent aggregates. Conversely, in apoptotic cells or in the presence of mitochondrial dysfunction, the loss of ΔΨm prevents the dye from accumulating and JC-1 remains in a monomeric form, characterized by green fluorescence. Therefore, the ratio of red/green fluorescence can be used as a tool to monitor mitochondrial function and apoptotic processes (45).

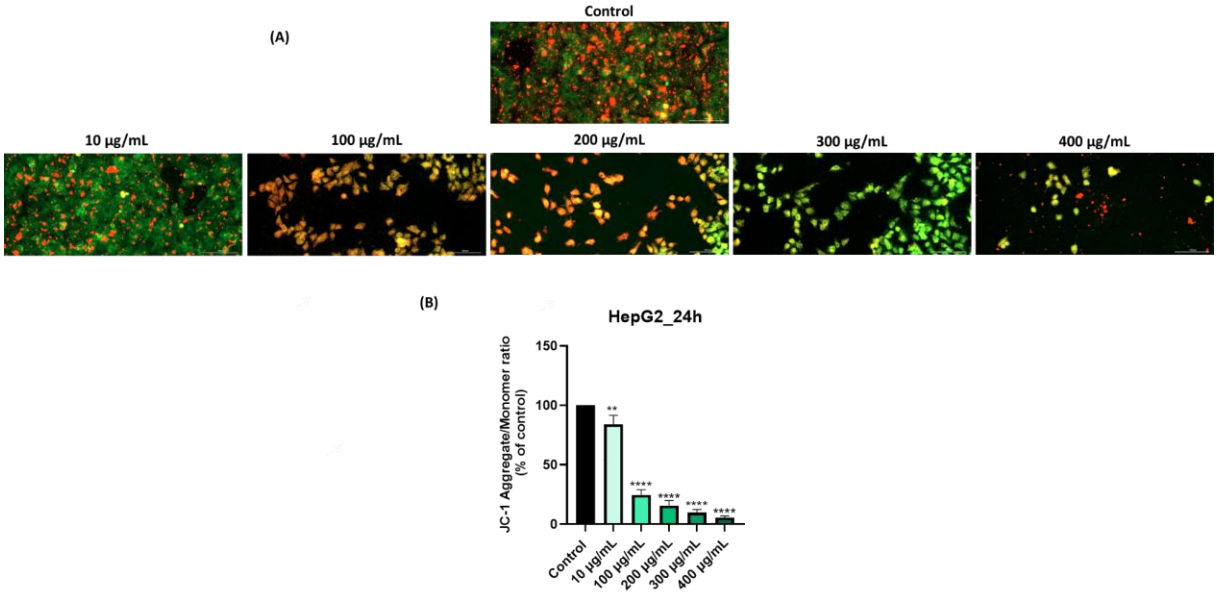

Figure 7.

Effects of the MCS@OA/PBS sample based on Fe_3O_4-NPs coated with a double layer of oleic acid and dispersed in PBS on the mitochondrial membrane potential of HepG2 cells following 24 h of exposure, as assessed by the JC-1 assay. (A) Representative fluorescence microscopy images acquired after JC-1 staining. Scale bar indicates 100 µm. (B) Quantitative analysis of the JC-1 aggregate-to-monomer fluorescence ratio. The results were expressed as a percentage relative to the untreated control. Data are presented as the mean ± standard deviation (SD). Statistical analysis was achieved using one-way analysis of variance (ANOVA), and then Dunnett's multiple comparison test was performed. Differences were considered statistically significant compared to the untreated control at the significance levels ** $p < 0.01$ and ****$p < 0.0001$

Following the JC-1 assay, a concentration-dependent decrease in mitochondrial membrane potential was detected upon exposure to MCS@OA/PBS. The decrease in ΔΨm observed in this study is in line with previous reports on Fe_3O_4-based nanomaterials. In ovarian cancer cells, self-assembled Fe_3O_4-based nanocomposites triggered mitochondrial membrane depolarization, a point confirmed by a decrease in the fluorescence of JC-1 aggregates and an enhancement in the fluorescence of JC-1 monomers. These results suggest that mitochondrial dysfunction may be one of the mechanisms behind the cytotoxicity induced by nanoparticles (46). Similar effects were shown in BEL-7402 hepatocellular carcinoma cells. In this cell line, exposure to Fe_3O_4-based magnetic nanoparticles at concentrations between 0.05 and 1 mg/mL over 24 hours significantly reduced ΔΨm, implying that mitochondrial impairment is an initial event in nanoparticle-mediated apoptosis (38). Du *et al*. also found that, when U2OS and Saos-2 osteosarcoma cell lines were treated for 48 hours with supramagnetic Fe_3O_4 nanoparticles at a concentration of 100 µg/mL, JC-1 staining clearly showed a significant drop in ΔΨm. This effect was further supported by the predominance of green fluorescence (47).

Analysis of Nuclear and Mitochondrial Aspects Using Fluorescence Staining

To analyze in more detail the effects of MCS@OA/PBS treatment at the subcellular level, HepG2 cells were stained with a double fluorescent dye, with Hoechst 33342 to assess the nuclear morphology and MitoTracker™ Red CMXRos to visualize the mitochondrial network. As reported in Figure 8, at the nuclear level, HepG2 cells in the control group showed a typical morphology, with oval nuclei and chromatin distributed uniformly. Cells treated with 10 µg/mL of MCS@OA/PBS showed nuclear characteristics comparable to those of the control group. Instead, starting from 100 µg/mL, the changes became concentration-dependent, with chromatin condensation, an increased number of rounded nuclei, a progressive decrease in density, and a reduction in nuclear size. These changes became more pronounced as the nanoparticle concentration increased (300–400 µg/mL), leading to wide nuclear damage characterized by a severe loss of nuclear integrity.

In the control group, HepG2 cell mitochondria exhibited a well-organized mitochondrial network (Figure 8). The mitochondrial morphology was similar in cells treated with 10 µg/mL of MCS@OA/PBS. At 100 µg/mL, concentration-dependent changes were observed, including increased mitochondrial fluorescence and mitochondrial fragmentation in a round shape and a gradual decrease in mitochondrial size. These effects became more prominent as the nanoparticle concentration went up, pointing to a destruction of the overall structure of the mitochondrial network.

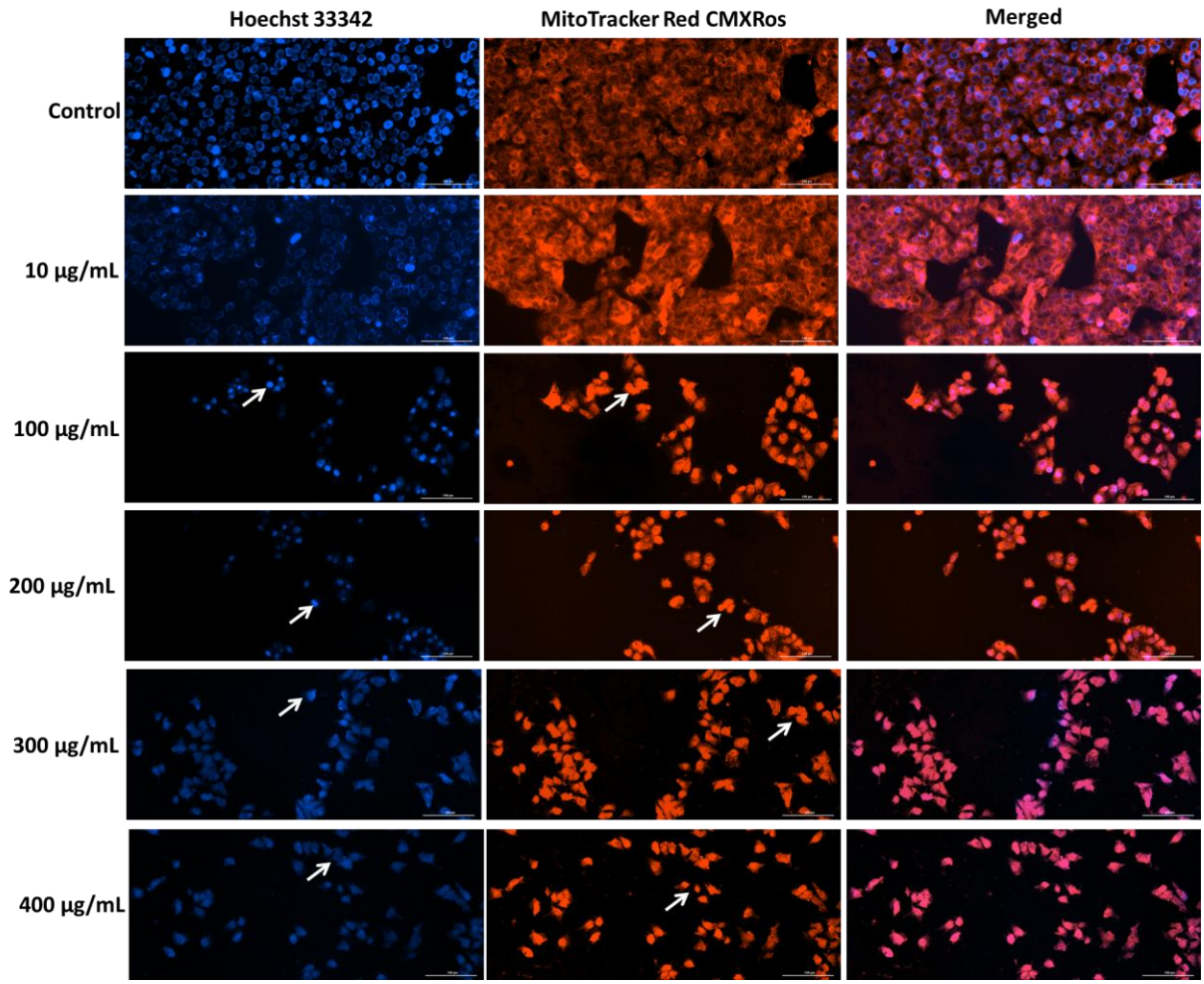

Figure 8.

Representative fluorescence microscopy images of HepG2 cells treated with the MCS@OA/PBS sample based on Fe_3O_4-NPs coated with a double layer of oleic acid and dispersed in PBS at concentrations ranging from 10 to 400 µg/mL. The scale bar represents 100 µm

Hoechst 33342 is one of the most commonly used fluorescent dyes for DNA staining in living cells. It allows the evaluation of nuclear morphology and chromatin organization by fluorescence microscopy and is thus a valuable tool to assess cellular responses to different treatments (48). The evaluation of nuclear morphology in this work showed concentration-dependent changes following exposure to MCS@OA/PBS. At 100 µg/mL, chromatin condensation and nuclear rounding were observed in the HepG2 cells, while treatment with the highest concentrations (300 and 400 µg/mL) caused significant nuclear damage, characterized by nuclear fragmentation. Moacă *et al*. assessed Fe_3O_4 nanoparticles containing an extract of *Artemisia absinthium* L. on the A375 melanoma cell line at concentrations up to 500 µg/mL for 72 h. They evaluated nuclear morphology after treatment using DAPI staining, showing that these nanoparticles induced apoptotic-like morphological changes similar to those observed in the present study (24).

At the same time, MitoTracker™ dyes are used to assess mitochondrial morphology, as they preferentially stain active mitochondria, allowing visualization of the mitochondrial network and its structural integrity. This analysis is crucial to comprehending the cellular mechanisms underlying cell death, especially since mitochondria play an important role in regulating apoptosis (21). In this study, starting at a concentration of 100 µg/mL, concentration-dependent alterations in mitochondrial architecture were detected, including rounding and fragmentation of the mitochondria, as well as a reduction in their size. These changes became gradually more pronounced as the concentration increased. Similar results were also reported for normal renal epithelial cells (Vero) treated with formulations based on magnetic iron oxide nanoparticles. After 24 hours of exposure to concentrations of 1, 3, and 5 µg/mL, slight changes were observed at the lowest concentration. However, increasing concentrations led to cell condensation, lower confluence, and more visible morphological changes (14).

Although the biological effects observed in the present study are attributed to the MCS@OA/PBS formulation, the possible contribution of the oleic acid coating should also be considered. Previous studies have shown that oleic acid can influence mitochondrial dynamics and cell viability in HepG2 cells, although these effects are less pronounced than those induced by saturated fatty acids such as palmitate (49,50).

To summarize, the results of this study confirm the potential of the MCS@OA/PBS sample as a cytotoxic agent against HepG2 cells. However, this study represents a preliminary *in vitro* investigation and has several limitations. Future studies should include testing the sample on normal hepatic cell lines to evaluate its safety profile and investigating a broader range of concentrations to determine the IC_{50} value (51). In addition, the exposure time could be extended to 48 and 72 hours to determine whether the observed effects become more pronounced over time. Although two-dimensional (2D) HepG2 cell cultures represent an important starting point for preliminary cytotoxicity assessment, they do not fully reproduce the physiological characteristics of human liver tissue. Therefore, future studies should investigate the biological activity of the MCS@OA/PBS sample using three-dimensional (3D) liver models, which better mimic the native tissue microenvironment.

In addition, because the treatment suspensions were prepared by direct dilution of the original MCS@OA/PBS stock suspension, the proportion of the suspension in the culture medium increased with the tested concentration, reaching approximately 12.35% (v/v) at the highest concentration. Therefore, a possible contribution of the dispersion medium to the observed biological effects at the highest concentration cannot be completely excluded. Future studies should include appropriate vehicle controls to further validate these findings.

Further studies should also include *in ovo* assays to evaluate irritation potential and effects on angiogenesis, followed by *in vivo* experiments in appropriate animal models to confirm the antitumor efficacy and safety of the formulation (52).

Finally, although the observed cytotoxic effects were associated with alterations in cell viability, lysosomal integrity, nuclear morphology, mitochondrial morphology, and mitochondrial membrane potential, the precise molecular mechanisms responsible for these effects remain to be elucidated. Recent studies have complemented morphological and viability assessments with the evaluation of apoptosis- and proliferation-related molecular markers, providing deeper mechanistic insights into the cytotoxic effects of anticancer agents. Therefore, future investigations should include the assessment of apoptosis- and proliferation-related markers, such as BAX, BCL-2, caspases, Ki-67, PCNA, and other signaling pathways involved in programmed cell death and cell proliferation, to better clarify the mechanisms underlying the biological activity of the MCS@OA/PBS sample (53).

Conclusions

Liver cancer remains one of the most significant global health challenges due to its high incidence and poor prognosis. Despite recent advances, current treatment options remain limited in their benefits, highlighting the need to develop more effective and safer treatment strategies.

The preliminary physicochemical characterization of the as-prepared MCS@OA/PBS suspension revealed a nanoscale Z-average hydrodynamic diameter, moderate PDI, satisfactory colloidal stability in PBS, and a measurable field-dependent magnetic response. However, because only a virgin magnetization curve was recorded, coercivity, remanence, and the magnetic classification of the formulation could not be established. Based on these physicochemical characteristics, the biological evaluation evidenced that the MCS@OA/PBS sample consisting of Fe_3O_4 nanoparticles coated with a double layer of oleic acid and dispersed in PBS exerts a pronounced cytotoxic effect against the HepG2 cell line. Treatment significantly reduced cell viability and induced concentration-dependent alterations in lysosomal integrity and nuclear morphology, as well as mitochondrial appearance and membrane potential, indicating significant cellular alterations.

Overall, these findings support the further investigation of the MCS@OA/PBS sample for HCC-related biomedical applications. However, the intrinsic concentration-dependent cytotoxicity observed in the present study highlights the need to define an appropriate concentration range before considering its application as a magnetically guided drug delivery platform.

Acknowledgement

The authors would like to thank "Victor Babeș" University of Medicine and Pharmacy Timișoara for supporting the experimental activities conducted in this study.

Funding

This work was supported by a grant from the Ministry of Research, Innovation and Digitization, CNCS-UEFISCDI, project number PN-IV-P2-2.1-TE-2023-1941, within PNCDI IV.

Availability of data and materials

The data generated in the present study are included in the figures and/or tables of this article.

Ethics approval and consent to participate

Not applicable.

AI use disclosure

During the preparation of this manuscript, the authors used QuillBot for language improvement, including spelling, grammar, clarity, and readability. The authors reviewed and revised all outputs from these tools and took full responsibility for the final content of the work.

Conflict of interest

The authors declare no conflict of interest.

References

1. International Agency for Research on Cancer. Global Cancer Observatory: cancer today [Internet]. Lyon: IARC; 2026 [cited 2026 May 01]. Available from: https://gco.iarc.who.int/today
2. Feng F, Zhao Y. Hepatocellular carcinoma: prevention, diagnosis, and treatment. Med Princ Pract. 2024;33(5):414-423.
3. Sadrinasab S, Saket S, Pourmohammadi N, Khosravi F, Fakhr MS. Modern therapeutic approaches for hepatic tumors: progress, limitations, and future directions. Discov Oncol. 2025;16(1):959.
4. Cai Y, Wang W, Jiao Q, Hu T, Ren Y, Su X, et al. Nanotechnology for the diagnosis and treatment of liver cancer. Int J Nanomedicine. 2024;19:13805-13821.
5. Alili L, Chapiro S, Marten GU, Schmidt AM, Zanger K, Brenneisen P. Effect of Fe3O4 nanoparticles on skin tumor cells and dermal fibroblasts. Biomed Res Int. 2015;2015:530957.
6. Moacă EA, Mihali CV, Macașoi IG, Racoviceanu R, Șoica C, Dehelean CA, et al. Fe3O4@C matrix with tailorable adsorption capacities for paracetamol and acetylsalicylic acid: synthesis, characterization, and kinetic modeling. Molecules. 2019;24(9):1727.
7. Căpraru A, Moacă EA, Păcurariu C, Ianoș R, Lazău R, Barbu-Tudoran L, et al. Development and characterization of magnetic iron oxide nanoparticles using microwave for the combustion reaction ignition, as possible candidates for biomedical applications. Powder Technol. 2021;394:1026-1038.
8. Pop D, Buzatu R, Moacă EA, Watz CG, Cîntă-Pînzaru S, Barbu-Tudoran L, et al. Development and characterization of Fe3O4@carbon nanoparticles and their biological screening related to oral administration. Materials (Basel). 2021;14(13):3556.
9. Moacă EA, Watz C, Faur AC, Lazăr D, Socoliuc V, Păcurariu C, et al. Biologic impact of green synthetized magnetic iron oxide nanoparticles on two different lung tumorigenic monolayers and a 3D normal bronchial model-EpiAirway microtissue. Pharmaceutics. 2023;15(1):2.
10. Borcan F, Len A, Dehelean CA, Dudás Z, Ghiulai R, Iftode A, et al. Design and assessment of a polyurethane carrier used for the transmembrane transfer of acyclovir. Nanomaterials (Basel). 2021;11(1):51.
11. Nguyen MD, Tran HV, Xu S, Lee TR. Fe3O4 nanoparticles: structures, synthesis, magnetic properties, surface functionalization, and emerging applications. Appl Sci. 2021;11(23):11301.
12. Ianoș R, Păculescu A, Păcurariu C, Lazău I. Solution combustion synthesis and characterization of magnetite, Fe3O4, nanopowders. J Am Ceram Soc. 2012;95:2236-2240.
13. Bica D, Vékás L, Avdeev MV, Marinică O, Socoliuc V, Garamus VM, et al. Sterically stabilised water-based magnetic fluids: synthesis, structure, and properties. J Magn Magn Mater. 2007;311:17-21.
14. Neagu MC, Boia ES, Andrică PA, Cristea AM, Sasco D, Bob F, et al. Synthesis, characterisation and a preliminary in vitro evaluation of a magnetic nanoformulation on kidney Vero cell line. Farmacia. 2025;73(6):1493-1505.
15. Rinaldi C, Chaves A, Elborai S, He X, Zahn M. Magnetic fluid rheology and flows. Curr Opin Colloid Interface Sci. 2005;10(3-4):141-157.
16. Puenea G, Almăjan-Guță B, Chioibaș R, Macașoi I, Geamantan A, Dinu Ș, et al. Evaluation of oleanolic acid, doxorubicin and their association in the treatment of melanoma: enhanced efficacy and antiangiogenic potential. Farmacia. 2023;71(6):1295-1304.
17. Apostu A, Buzatu R, Cabuta M, Macasoi I, Dinu S, Iftode A, et al. In vitro assessment of the potential cytotoxic effect of metformin on colorectal cancer cells. Farmacia. 2023;71(1):50-57.
18. Breban-Schwarzkopf D, Danila AI, Tanase AD, Munteanu K, Haj Ali D, Popovici R, et al. Eugenol - a natural alternative in dentistry: an in vitro and in ovo biosafety assessment. Farmacia. 2024;72(5):1011-1018.
19. Marcovici I, Vlad D, Buzatu R, Popovici RA, Cosoroaba RM, Chioibas R, et al. Rutin linoleate triggers oxidative stress-mediated cytoplasmic vacuolation in non-small cell lung cancer cells. Life (Basel). 2024;14(2):215.
20. Nica DF, Cosoroabă RM, Dinu Ș, Dumitrel ȘI, Chioran D, Tănase A, et al. Exploring thymol's cytocompatibility and potential selective cytotoxicity in human primary gingival fibroblasts and pharyngeal carcinoma cells: an in vitro and in ovo investigation. Dent J (Basel). 2026;14(2):105.
21. Jupâneanț RA, Anton A, Bojincă M, Haj Ali D, Predescu IA, Păcurar AT, et al. In vitro insight into the potential of curcumin to enhance the sensitivity of A375 human melanoma cells to cisplatin. Farmacia. 2026;74(3):742-755.
22. Bhange M, Telange DR. Unlocking the potential of phyto nanotherapeutics in hepatocellular carcinoma treatment: a review. J Hepatocell Carcinoma. 2024;11:2241-2256.
23. Arzumanian VA, Kiseleva OI, Poverennaya EV. The curious case of the HepG2 cell line: 40 years of expertise. Int J Mol Sci. 2021;22(23):13135.
24. Moacă EA, Watz CG, Flondor DI, Păcurariu C, Barbu-Tudoran L, Ianoș R, et al. Biosynthesis of iron oxide nanoparticles: physico-chemical characterization and their in vitro cytotoxicity on healthy and tumorigenic cell lines. Nanomaterials (Basel). 2022;12(12):2012.
25. Boyer C, Whittaker MR, Bulmus V, Liu J, Davis TP. The design and utility of polymer stabilised iron oxide

nanoparticles for nanomedicine applications. NPG Asia Mater. 2010;2:23-30.
26. Estelrich J, Escribano E, Queralt J, Busquets MA. Iron oxide nanoparticles for magnetically-guided and magnetically-responsive drug delivery. Int J Mol Sci. 2015;16(4):8070-8101.
27. Medeiros SF, Filizzola JOC, Fonseca VFM, Oliveira PFM, Silva TM, Elaissari A, et al. Synthesis and characterization of stable aqueous dispersion of functionalised double-coated iron oxide nanoparticles. Mater Lett. 2015;160:522-525.
28. Shete PB, Patil RM, Tiwale BM, Pawar SH. Water dispersible oleic acid-coated Fe3O4 nanoparticles for biomedical applications. J Magn Magn Mater. 2015;377:406-410.
29. Li D, Jiang D, Chen M, Xie J, Wu Y, Dang S, et al. An easy fabrication of monodisperse oleic acid-coated Fe3O4 nanoparticles. Mater Lett. 2010;64:2462-2464.
30. Patil RM, Shete PB, Thorat ND, Otari SV, Barick KC, Prasad A, et al. Non-aqueous to aqueous phase transfer of oleic acid coated iron oxide nanoparticles for hyperthermia application. RSC Adv. 2014;4:4515-4522.
31. Anton N, Bally F, Serra CA, Ali A, Arntz Y, Mely Y, et al. A new microfluidic setup for precise control of the polymer nanoprecipitation process and lipophilic drug encapsulation. Soft Matter. 2012;8:10628-10635.
32. Lopes IMD, de Oliveira IM, Bargi-Souza P, Cavallin MD, Kolc CSM, Khalil NM, et al. Effects of silver nanoparticle exposure to the testicular antioxidant system during the prepubertal rat stage. Chem Res Toxicol. 2019;32(6):986-994.
33. de Oliveira IM, Cavallin MD, Corrêa DEDC, Razera A, Mariano DD, Ferreira F, et al. Proteomic profiles of thyroid gland and gene expression of the hypothalamic-pituitary-thyroid axis are modulated by exposure to AgNPs during prepubertal rat stages. Chem Res Toxicol. 2020;33(10):2605-2622.
34. Zhang L, He R, Gu HC. Oleic acid coating on the monodisperse magnetite nanoparticles. Appl Surf Sci. 2006;253(5):2611-2617.
35. Watz CG, Mihali CV, Oprean C, Krauss Maldea L, Tatu CA, Nicolov M, et al. Fe3O4@β-cyclodextrin nanosystem: a promising adjuvant approach in cancer treatment. Nanomaterials (Basel). 2025;15(15):1192.
36. Ghasemi M, Turnbull T, Sebastian S, Kempson I. The MTT assay: utility, limitations, pitfalls, and interpretation in bulk and single-cell analysis. Int J Mol Sci. 2021;22(23):12827.
37. Ebadi M, Rifqi Md Zain A, Tengku Abdul Aziz TH, Mohammadi H, Tee CAT, Rahimi Yusop M. Formulation and characterization of Fe3O4@PEG nanoparticles loaded sorafenib: molecular studies and evaluation of cytotoxicity in liver cancer cell lines. Polymers (Basel). 2023;15(4):971.
38. Kai W, Xiaojun X, Ximing P, Zhenqing H, Qiqing Z, Dandan J, et al. Cytotoxic effects and the mechanism of three types of magnetic nanoparticles on human hepatoma BEL-7402 cells. Nanoscale Res Lett. 2011;6:480.
39. Elmore S. Apoptosis: a review of programmed cell death. Toxicol Pathol. 2007;35(4):495-516.
40. American Type Culture Collection. Hep G2 (HEPG2) (HB-8065) [Internet]. Manassas (VA): ATCC; 2026 [cited 2026 May 01]. Available from: https://www.atcc.org/products/hb-8065
41. Sathishkumar G, Logeshwaran V, Sarathbabu S, Jha PK, Jeyaraj M, Rajkuberan C, et al. Green synthesis of magnetic Fe3O4 nanoparticles using Couroupita guianensis Aubl. fruit extract for their antibacterial and cytotoxicity activities. Artif Cells Nanomed Biotechnol. 2018;46(3):589-598.
42. Repetto G, del Peso A, Zurita JL. Neutral red uptake assay for the estimation of cell viability/cytotoxicity. Nat Protoc. 2008;3(7):1125-1131.
43. Boya P, Kroemer G. Lysosomal membrane permeabilization in cell death. Oncogene. 2008;27(50):6434-6451.
44. Jędrzejczak-Silicka M, Szymańska K, Mijowska E, Rakoczy R. The influence of graphene oxide-Fe3O4 differently conjugated with 10-hydroxycamptothecin and a rotating magnetic field on adenocarcinoma cells. Int J Mol Sci. 2024;25(2):930.
45. Sivandzade F, Bhalerao A, Cucullo L. Analysis of the mitochondrial membrane potential using the cationic JC-1 dye as a sensitive fluorescent probe. Bio Protoc. 2019;9(1):e3128.
46. Wei H, Li H, Yu D, Liu W, Dong S, Zhang X, et al. Apoptosis-induced treatment for ovarian cancer from self-assembled nanocomposites of Fe3O4 nanoparticles and porous organic cages. Colloids Surf A Physicochem Eng Asp. 2024;695:134070.
47. Du S, Li J, Du C, Huang Z, Chen G, Yan W. Overendocytosis of superparamagnetic iron oxide particles increases apoptosis and triggers autophagic cell death in human osteosarcoma cell under a spinning magnetic field. Oncotarget. 2017;8(6):9410-9424.
48. Grosu (Dumitrescu) C, Boță M, Bonțe D, Toma C, Smeu A, Vlaia L, et al. Myricetin-fisetin combinatorial treatment as a potential strategy for cutaneous melanoma - an in vitro study. Farmacia. 2025;73(2):477-486.
49. de Sousa IF, Migliaccio V, Lepretti M, Paolella G, Di Gregorio I, Caputo I, et al. Dose- and time-dependent effects of oleate on mitochondrial fusion/fission proteins and cell viability in HepG2 cells: comparison with palmitate effects. Int J Mol Sci. 2021;22(18):9812.
50. García-Ruiz I, Solís-Muñoz P, Fernández-Moreira D, Muñoz-Yagüe T, Solís-Herruzo JA. In vitro treatment of HepG2 cells with saturated fatty acids reproduces mitochondrial dysfunction found in nonalcoholic steatohepatitis. Dis Model Mech. 2015;8(2):183-191.
51. Tănase AD, Bojoga DE, Crăciunescu EL, Pop DM, Novac AC, Negruțiu ML, et al. Ethics and medical legislation in retrospective experimental studies. The role and importance of the legislative aspect. Rom J Oral Rehabil. 2024;16(1):298-306.
52. Tănase AD, Sinescu C, Petrescu EL, Pop DM, Novac AC, Negruțiu ML, et al. Ethical and legal considerations in research studies involving human embryos. Rom J Oral Rehabil. 2024;16(3):557-566.
53. Mederle AL, Semenescu A, Drăghici GA, Dehelean CA, Vlăduț NV, Nica DV. Sodium butyrate: a multifaceted modulator in colorectal cancer therapy. Medicina (Kaunas). 2025;61(1):136.